Detection module of the C-BORD Rapidly Relocatable Tagged Neutron Inspection System (RRTNIS)

F. Pino, C.L. Fontana, G. Nebbia, B. Pedersen, G. Varasano, A. Sardet, C. Carasco, B. Pérot, Arnaud Grivet Sébert, Jean-Philippe Poli, et al.

Detection module of the C-BORD Rapidly Relocatable Tagged Neutron Inspection System (RRTNIS)

F. Pino*[1], C.L. Fontana[1], G. Nebbia[2], B. Pedersen[3], B. Pedersen[3], G. Varasano[3], A. Sardet[4], C. Carasco[4], B. Pérot[4], A. G. Sebert[5], J. P. Poli[5], G. Sannié[5], A. Iovene[6], C. Tintori[6], P. Sibczynski[7], K. Grodzicki[7], L. Swiderski[7], and S. Moretto[1]

[1]Department of Physics and Astronomy "Galileo Galilei", University of Padova, Via Marzolo, 8, I-35131, Padova, Italy
[2]INFN Sezione Padova, Via Marzolo 8, I-35131, Padova, Italy
[3]Nuclear Security Unit, Directorate for Nuclear Safety & Security, Joint Research Centre, Via E. Fermi 2749, 21027 Ispra (VA), Italy
[4]CEA, DEN, Cadarache, Nuclear Measurement Laboratory, F-13108 Saint-Paul-lez-Durance, France
[5]CEA, DRT, LIST, Saclay, F-91191 Gif-Sur-Yvette, France
[6]CAEN S.p.A., Via Vetraia, 11, Viareggio LU 55049, Italy
[7]National Center for Nuclear Research, ul. Andrzeja Soltana 7, Otwock-Swierk 05-400, Poland

Abstract

This article reports a detailed description of the integration tests of the first Rapidly Relocatable Tagged Neutron Inspection System (RRTNIS) carried out at the European Commission's Joint Research Centre in Ispra (Italy). This technology allows the detection and identification of suspicious or illicit materials (such as narcotics, explosives,

*Corresponding author: Tel: +39 049 827 5934, felixpino@gmail.com

contraband goods, etc.) inside a cargo container using active neutron interrogation, with the so-called associated particle technique. The method is based on the measurement of the gamma photons emitted by the de-excitation of nuclei that undergo, mainly, inelastic scatterings with incident fast neutrons ($E_n \sim 14$ MeV). A set of scintillation detectors (NaI:Tl and $LaBr_3$:Ce) is employed to perform gamma spectroscopy. The data acquisition system is based on fast signal digitizers and customized data acquisition software. A general technical description of the detection module and an outline of the data acquisition system (DAQ) are given. Also, we present the results of the integration tests, in particular, some examples of the performance of the system in the laboratory are shown, specifically, when using no target (background measurement) and when using mono-elemental and an explosive simulant target. Obtained results suggest that all technical requirements are achieved, and the next step will be the field trials.

Keywords: Tagged Neutron Inspection System ; Active Neutron Interrogation ; Digital Pulse Processing ; Homeland Security

1 Introduction

C-BORD (effective Container inspection at BORDer control points) is a European H2020 (Research and Innovation Program) project [1, 2, 3, 4, 5, 6, 7, 8] aimed to develop, and test, a comprehensive cost-effective solution for the inspection of large-volume freight against illicit trafficking. The procedures that have to be followed in order to open suspect containers are time-consuming and expensive, for economical and safety reasons, hence the project is focused on Non-Intrusive Inspection (NII) techniques. In order to protect EU borders, the project addresses a wide range of NII targets in containers: including explosives, chemical warfare agents, illicit drugs, contraband goods and special nuclear materials. The main technical objective of C-BORD is to develop a toolbox of first-line & second-line devices, employing different non-destructive passive and active techniques: advanced radiation portal monitors, next generation cargo X-ray, tagged neutron inspection, photofission and evaporation based detection. The development of a unique graphical user interface (GUI) for all systems aims at improving the quality of the interpretation and decision making. The software guarantees the data fusion between the sub-systems, with decision support software and a common data format. In the C-BORD framework, the Rapidly Relocatable Tagged Neutron Inspection System (RRTNIS) is conceived as a second-line inspection tool. The RRTNIS is to be used on sealed containers in order to detect explosives, illicit drugs and chemical agents, in specific voxels (ele-

mentary volume units); previously identified as suspect by the first-line scan sub-systems (e.g. X-ray scan). X-ray radiography is not effective in distinguishing materials with similar densities and atomic numbers; whereas the tagged neutron inspection helps distinguishing organic substances (explosives vs. narcotics vs. benign materials). The scope of the RRTNIS is to offer better performance with respect to the former system, which was a large and fixed portal developed on the frame of EURITRACK project [9, 10, 11].

The core of the RRTNIS design is the neutron generator. Fast neutrons (E_n = 14 MeV) are produced using the D-T reaction ($D + T \rightarrow n + \alpha$). The associated alpha particles tag in time and direction the neutrons emitted, more details in [12, 13]. The neutron generator is encased in a polyethylene shielding to ensure radiation protection. The tagged neutron beam exits the polyethylene shielding through a conical hole, with a total aperture angle of 20°. Neutrons interact with the materials they encounter, mostly by inelastic scattering with the nuclei. Characteristic de-excitation gamma rays are emitted in all directions by the nuclei. Using a properly designed detection module one can record: the energy spectrum of the photons emitted and the alpha-gamma time-difference distribution. The time-difference, between the alpha and the detection of the neutron-induced gamma, allows us to determine the neutron Time-of-Flight (ToF), and subsequently its position of interaction. By selecting a region of interest (ROI) on the ToF vs. direction distribution, one can obtain the energy spectrum of the gamma photons, emitted from any voxel in the container. Finally, the relative proportion of elements in the voxel of interest can be obtained by unfolding the gamma spectrum into a linear combination of the spectra relating to each element [5]. With this information it is possible to perform a general material classification (organic, ceramic, etc.). A finer identification can also be performed, for instance in organic materials, to distinguish between illicit drugs, explosives, and benign materials, by applying a fuzzy decision tree method [6]. Respect to prior systems the main innovations of the C-BORD RRTNIS are: it is a rapidly relocatable system (no large fixed portal like EURITRACK system), it has a compact neutron generator shielding (no fixed concrete walls as in EURITRACK), so, the limited restricted area is shorter, the neutron generator capabilities are extended (higher neutron emission rate, compact design, efficient tagging), the digital nuclear electronics is more compact and its setup is done in a very efficient way, high resolution gamma-ray scintillators ($LaBr_3$:Ce) have been added to the detection system in order to improve the identification of suspicious materials (possibility to detect chemical agents), and elements of artificial intelligence have been included in order to assist the analysis of the measurements.

In this work we thoroughly describe the detection module of the RRT-

NIS; giving a general technical description of the set of scintillation detectors, an outline of the data acquisition system (DAQ). Also, we present the results of the integration tests carried out at the European Commission's Joint Research Centre in Ispra (Italy), in particular the mechanical integration (assembly of the polyethylene radiological shield, placement and alignment of the neutron generator, positioning of the detectors and lead shield on the frame) and the electronic integration (connection of all detectors with the electronic units and configuration of the acquisition system). To test the performance of the whole system, ToF spectra with and without target (background) are analyzed, and a few pure elements responses are obtained in order to contribute with the building of the elemental database. Finally, an explosive simulant (RDX simulant) spectrum was acquired, showing that each pure element contained was identified.

2 Experimental details

2.1 Description of the RRTNIS detection module

The detection module of the RRTNIS can be divided into two parts: the scintillation detector array and the data acquisition system (read-out electronics and data acquisition software).

2.1.1 Scintillation detectors

The detector array consists of twenty (20) large-size (5" × 5" × 10" parallelepiped-shaped) NaI:Tl detectors, and four (4) 3" × 3" cylindrical $LaBr_3$:Ce detectors. The detectors are mounted on an iron frame (in a backscatter configuration, see Figure 1) which includes a lead shield to reduce mainly the recording of gamma, coming from neutron capture reactions on hydrogen in the polyethylene shielding. NaI:Tl detectors were assembled and used in order to achieve the main requirements of the project [3]. $LaBr_3$:Ce detectors are intended for chemical warfare detection, especially for the recognition of specific elements like arsenic (As) and bromine (Br) that emit characteristic neutron-induced gamma rays at low energy [14], i.e. less than 500 keV, which are difficult to resolve with the NaI:Tl detectors (energy resolution of the large-size NaI:Tl scintillators at E $\leq$ 500 keV is $\sim$ 10 %). A study to select the best photomultiplier tube (PMT) to be coupled with the NaI:Tl crystals was performed (details in [1, 2]). The chosen PMT is the Hamamatsu R11833-100HA together with an active voltage divider. The energy resolution achieved is around 8% (at 662 keV), time resolution $\sim$ 2 ns (at threshold level $\sim$1 MeV), linearity and gain stability up to counting rates $\sim$

250 $\times 10^3$ s^{-1} (kilo counts-per-second) for all NaI:Tl detectors. Being large volume crystals, the effect of the gamma photon interaction position on the time and energy resolution was studied. The energy resolution was found to be almost unaffected, while the variation of the time resolution was less than 5% with respect to the whole average detector response [1].

Of the four available $LaBr_3$:Ce detectors for the project, only two were used for the tests presented in this work. The two 3"×3" $LaBr_3$:Ce crystals were coupled to Hamamatsu R10233-100-01 photomultipliers, which is an assembly PMT model specially designed for this kind of crystal with very high light output. $LaBr_3$:Ce detectors exhibited energy resolution ∼3.5% (at 662 keV), time resolution <0.6 ns (threshold ∼1 MeV), good linearity and gain stability up to 140×10^3 s^{-1} [2].

2.1.2 Data acquisition unit

The electronics for nuclear signal processing consists of a compact unit based on fast signal digitizers. It is composed of:

- Two CAEN V1730 VME Digitizers, 16 ch, 14 bit, 500 MS/s (with a Digital Constant Fraction Discriminator, DCFD, embedded in the firmware for precise timing measurements);
- Five CAEN V6533 VME HV supply, 6 ch (NEG), 4 kV/3 mA;
- One CAEN V2718 VME-PCI Optical Link Bridge.
- Optical fiber connections using the CAEN CONET2 protocol for fast acquisition (CAEN A3818 PCI Express CONET2 Controller).

A computer with a custom-made data acquisition software called ABCD (Acquisition and Broadcast of Collected Data) [15, 16, 17] completes the data acquisition unit. In the spirit of the open-access philosophy of the H2020 funded research, ABCD was released as an open-source project*. Figure 2 shows the layout of the complete RRTNIS detection module.

The data acquisition system has been configured to treat both digitizers as independent modules with no synchronization between them. Each digitizer internally validates the acquired signals only if it detects a coincidence between the alpha signals (X, Y and SUM signals coming from the YAP:Ce detector) and at least one of the gamma detectors. Signals that are not validated are discarded. Figure 2 shows details of the connection scheme.

*The source code is available at the official repository: https://gitlab.com/cristiano.fontana/abcd

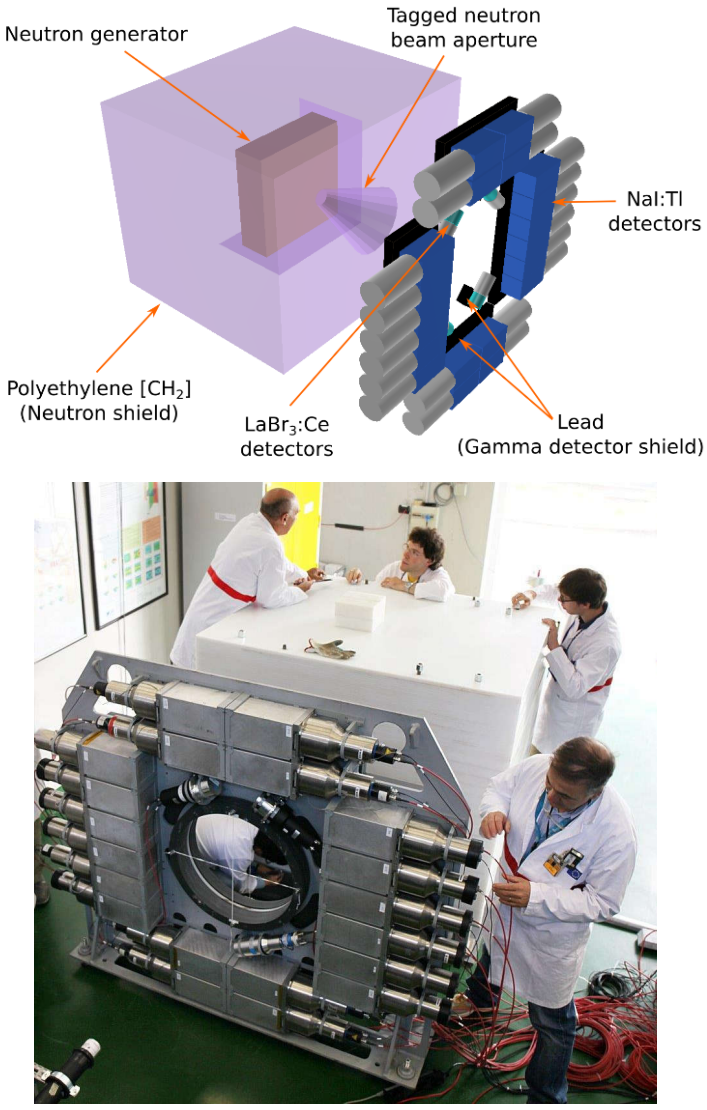

Figure 1: Schematic representation (a) and picture (b) of the RRTNIS parts during the integration tests at JRC.

RRTNIS diagram

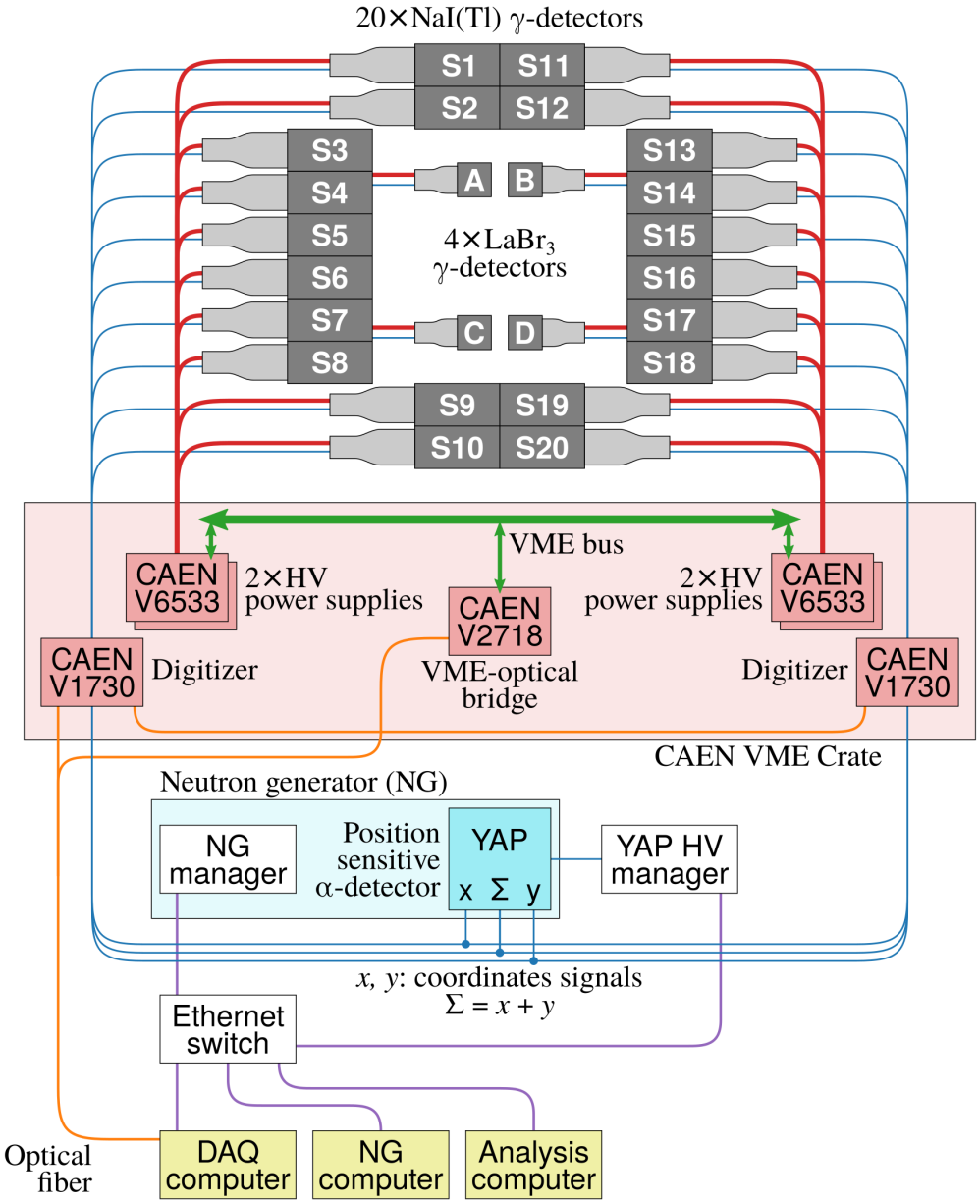

Figure 2: Schematic representation of the connections between the components of the RRTNIS detection module.

X, Y and SUM signals, coming from the YAP:Ce detector, are also used to build the so-called alpha XY map. This is a 2D plot ("X direction" versus "Y direction") that shows the interaction position of the alpha particles in the scintillator. Assuming equal gain, "X direction" ("Y direction") is equal to the X signal (Y signal) total integral to SUM signal total integral. According to this convention, "X direction" and "Y direction" equal to 1 correspond to an event that interacts in the center of the YAP:Ce crystal.

With such configuration, and a neutron emission rate of 7×10^7 s^{-1}, the system collects around 4×10^5 Events/s per digitizer (all channels). The DAQ was proven to be able to sustain rates of up to 4×10^5 Events/s in similar conditions, with a dead time of 1% [15, 16]. As far as the laboratory test described in this manuscript, the neutron inspection time was not a key issue (normally 30 min was enough to obtain good statistics spectra). In a future paper, the field neutron inspection times will be better defined. The system produces around 700 MB/min of data during a neutron inspection.

After the filtering by means of the digitizer validation, it is possible to pre-process the data. During the acquisition, partial results are displayed on-line (e.g. waveforms visualization, energy and ToF spectra calculation for each channel, etc.). This preprocessing is useful to monitor the performance of each of the system's elements. The filtered data are saved in a binary format containing channel, timestamp and energy information for each detected event. The analysis of the data, presented in this work, was performed in offline mode. First, detectors are calibrated in time and energy, then, a particular direction of the neutron beam is selected, by defining an ROI on the alpha XY map. Afterward, the data are merged to create only one aggregated spectrum per detector kind (NaI:Tl and $LaBr_3$:Ce). Results given in this work are processed until this step. In a real neutron inspection, an unfolding procedure is applied to the aggregated spectra, employing the mono-elemental database. The fractions of elements of the analyzed voxel can be identified by means of the unfolded analysis; more details about the data processing can be found in [5]. Finally, artificial intelligence methods are applied to classify the voxel material and, possibly, to identify a threat material. In particular the approach is the fuzzy decision tree; more detail is given in [6].

2.2 Integration test

The integration tests consisted, firstly, in doing the mechanical integration of the system, i.e., assembly of the polyethylene radiological shield, placement and alignment of the neutron generator and positioning of the detectors and lead shield on the iron frame. Secondly, in doing the electronic integration

of the detection module, that includes the connection of all detectors with the electronic units (power supply and digitizers) and the configuration of the DAQ (set-up of the logical treatment of the signals). The dimensions of the polyethylene box is 130 × 154 × 150 cm^3 with a cavity inside (to place the neutron generator) that allows to have a 40 cm of thickness wall. The associated particle neutron generator is an specific model (GENIE TPA17 CBORD) produced by Sodern (France). It produces a maximum neutron emission rate of 10^8 s^{-1}. The alpha detector for neutron tagging (timing and neutron direction definition) is a YAP(Ce) scintillator (49 mm diameter) coupled to a multi-anode photomultiplier (Hamamatsu H8500). The output consists in 3 analog outputs (X direction, Y direction and SUM) for alpha positioning and timing. For the alignment of the neutron generator, a cylindrical liquid organic scintillator (50 mm diameter × 50 mm thickness), EJ-309 type from Eljen Technology, was used as a neutron counter [18, 19]. Since the main scope of this work was to perform the integration of the detection module of the RRTNIS and to start the building of the mono-elemental database, the samples used during the tests were some kilograms of: graphite (C), water (O), silicon (Si), aluminum (Al) and few tens of kilograms of nitrogen (N), iron (Fe), copper (Cu) and Royal Demolition eXplosive (RDX) simulant ($Si_3C_3H_6N_6O_6$). The measurement time of each run was set in 30 min, that allows us to get good statistics spectra.

3 Experimental results

3.1 Neutron generator and spatial resolution

In order to perform the measurements for the alignment of the neutron generator, the EJ-309 scintillator was fixed to a base movable along a guide rail. The movements (change of position and speed) were controlled from an embedded computer using the LinuxCNC platform [20, 21]. Same DAQ mentioned on Section 2.1.2 was used to acquire the neutron counter and the YAP:Ce detector (X, Y and SUM) signals. In Figure 3a, the alpha map corresponding to all YAP signals acquired in one measurement is shown. The nonlinearity of position reconstruction on the edges of the alpha map is due to incomplete YAP scintillation light collection. Such a distortion has an impact on the transformation of the YAP coordinates to the true neutron direction, but only with the alpha events on the edges, because at the center of the YAP map there is linearity. On the other hand, in Figure 3b the alpha map built with the YAP signals which are in coincidence with the neutron counter events is given. As can be seen, such a measurement allows the

direction in which the neutrons were emitted to be reconstructed and, as a consequence, this can be used as a guide to fine-tune the polar angle direction of the neutron generator. The azimuth direction was fixed by the mechanical holder. Besides, Figures 3c and 3d show the X and Y direction projections of Figure 3b. The neutron counter was located in front and on the conical beam axis, at 2 m from the neutron generator. Most of the events in Figure 3b correspond to alpha particles that interact with the central part of the YAP:Ce crystal, as expected when the neutron generator is properly aligned.

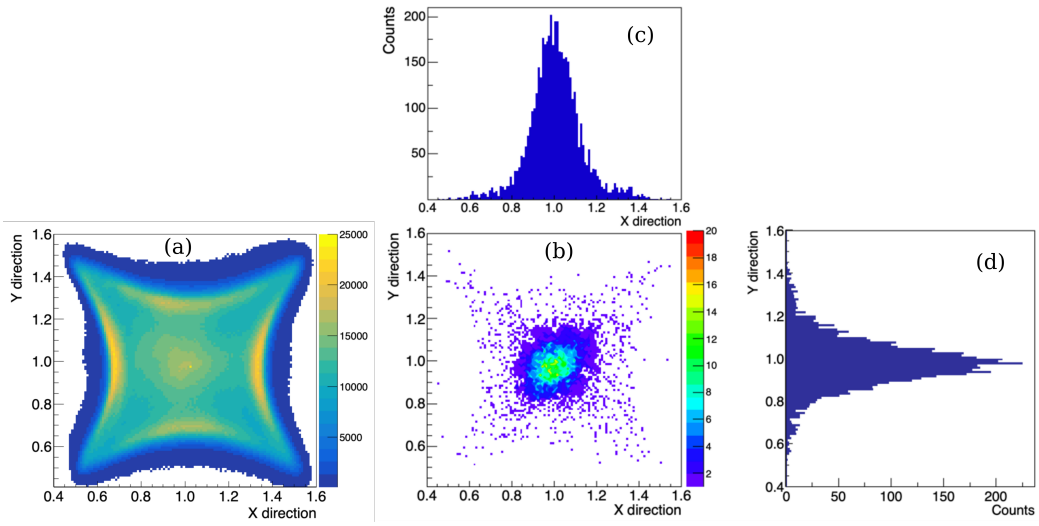

Figure 3: Alpha map, single alpha counts (a) and alpha/neutron coincidences (b), obtained when the neutron detector was located in front and on the axis of the beam cone, showing a proper alignment of the neutron generator. X (c) and Y (d) direction distributions are also shown.

As a way to estimate the spatial resolution (regarding X and Y directions) achieved with the system, another measurement with the neutron counter was considered. Using the LinuxCNC platform, the neutron counter was displaced one meter along a direction perpendicular to the neutron beam axis, considering Z direction as the beam axis, and X direction as the movement line of the neutron counter. The distance between the counter and the neutron generator was 2 m (when the counter was centered). The speed was set at 100 mm/min. Event data saved by the digitizer allow to extract part of the time history of the whole measurement, for example, selecting only 30 seconds of acquisition, the alpha map corresponding to a displacement of 50 mm is obtained. Considering the dimension of the neutron counter, one obtains a representation of the alpha map when an area of 100 mm x 50 mm is inspected (at 2 m from the neutron generator). By following this proce-

Table 1: Standard deviation of the X direction distribution and radius of the lighted up circle on the YAP crystal corresponding to several neutron counter displacements.

Displacement (mm)	Inspected area (mm^2)	σ (mm) ± 0.1
200	250 × 50	4.4
150	200 × 50	4.2
100	150 × 50	4.0
50	100 × 50	3.8
25	75 × 50	3.8

dure, the standard deviation (σ) values of the X and Y distributions can be studied as a function of the selected displacement. Arbitrary units of X and Y direction can be calibrated into length units (mm) by assuming that their total range must be 49 mm (dimension of the YAP:Ce crystal). The results extracted from the projection of the alpha map on the abscissa (X direction distribution) are given in Table 1. Sigma (σ) values of Y distributions were found to be almost constant $\sim$ 3.9 mm.

A slow decrease of the σ as the displacement of the neutron counter becomes shorter can be observed from the results given in Table 1, however, a minimum constant value ($\sim$ 3.8 mm) is observed even when the displacement is reduced, meaning that 10 cm is the spatial resolution value of the alpha detector. Therefore, taking into account the dimension of the neutron counter (50 mm dia.), the corresponding inspected area could be pictured as a square with an edge $\sim$ 10 cm. Z direction resolution can be estimated using the time resolutions of both kinds of detectors, and keeping in mind the speed of 14 MeV neutrons ($\sim$ 5 cm/ns). In consequence, the spatial resolution in Z direction is $\sim$ 10 cm and $\sim$ 3 cm when using events acquired with NaI:Tl and $LaBr_3$:Ce detectors respectively.

3.2 Time-of-flight spectrum and background

The gamma-ray events detected in coincidence with the X, Y and SUM signals are saved during the measurement into a file. Taking into account the digital constant fraction discrimination delay, the cable length and the range of interest of the neutron flight path, the coincidence gate was set to 400 ns. A Time-of-Flight (ToF) spectrum is calculated for each detector (see Figure 4), in order to determine the sample position. The alpha map allows a selection of the neutrons emitted in the direction of the sample (see

Figure 4a) located on the axis of the beam cone, because in field tests the suspicious voxel to be inspected will be aligned with the cone beam, thanks to appropriate mechanical positioning of the RRTNIS. Figures 4b and 4c show the data merged of two NaI:Tl and two $LaBr_3$:Ce detectors (one for each digitizer, which correspond to one for each side of the detector array, see S6 and S16 in Figure 2). Figure 4 shows measurements of a target and of the active background (without target). In Figures 4b and 4c the ToF has been converted to a position along the tagged neutron beam axis (distance in m with respect to the neutron generator) by taking as a reference the position of the detector frame. By selecting the events belonging to a ToF (or distance) interval, it is possible to get the energy spectrum of the neutron-induced gamma rays corresponding to the voxel of interest.

By inspecting the ToF spectra without alpha selection (see Figures 4b and 4c), firstly, a constant background (due to random coincidences) can be seen at negative positions. Then, a small distribution of events, between 0 and 0.8 m, produced by the interaction of neutrons with the polyethylene radiological shielding are identified. Later on, at ~ 1 m, gamma rays coming from the lead shield and holder of the detectors start to be important (correlated background). For both kinds of detector, this distribution reaches its maximum at 1.15 - 1.2 m and has a very long tail. Over those events and the constant background, a peak of events coming from a target is recognized (if the target is present). And finally, at around 4 m the events belonging to a beam dump wall (already present in the facility) are seen.

Also in Figures 4b and 4c the effect of the alpha map selection on the ToF spectra is shown, for NaI:Tl and $LaBr_3$:Ce detectors respectively. It is worth noting that the recognition and the determination of the position of the sample is enhanced after the alpha map selection procedure. Background (random and correlated) and events produced by the interaction of neutrons with the polyethylene are highly reduced with respect to the target peak intensity. The better timing performance of the $LaBr_3$:Ce detectors, with respect to the NaI:Tl ones, is evident on the ToF spectra, both with and without alpha selection. The Full Width at Half Maximum (FWHM) obtained for the time distributions (with alpha selection) shown in Figures 4b and 4c are (4.65 ± 0.07) ns (NaI:Tl) and (3.4 ± 0.1) ns ($LaBr_3$:Ce), which correspond to a neutron flight path FWHM of (20.5 ± 0.5) cm and (15.4 ± 1.0) cm, respectively. Furthermore, looking at the correlated background events on the ToF spectra without alpha selection, it is possible identify three peaks corresponding to the obstacles on the beam path (identification done further with Figures 5 and 6 give, from left to right: lead shield, detector frame and target) in Figure 4c with $LaBr_3$:Ce detectors, while only two peaks can be seen in Figure 4b with NaI:Tl detectors.

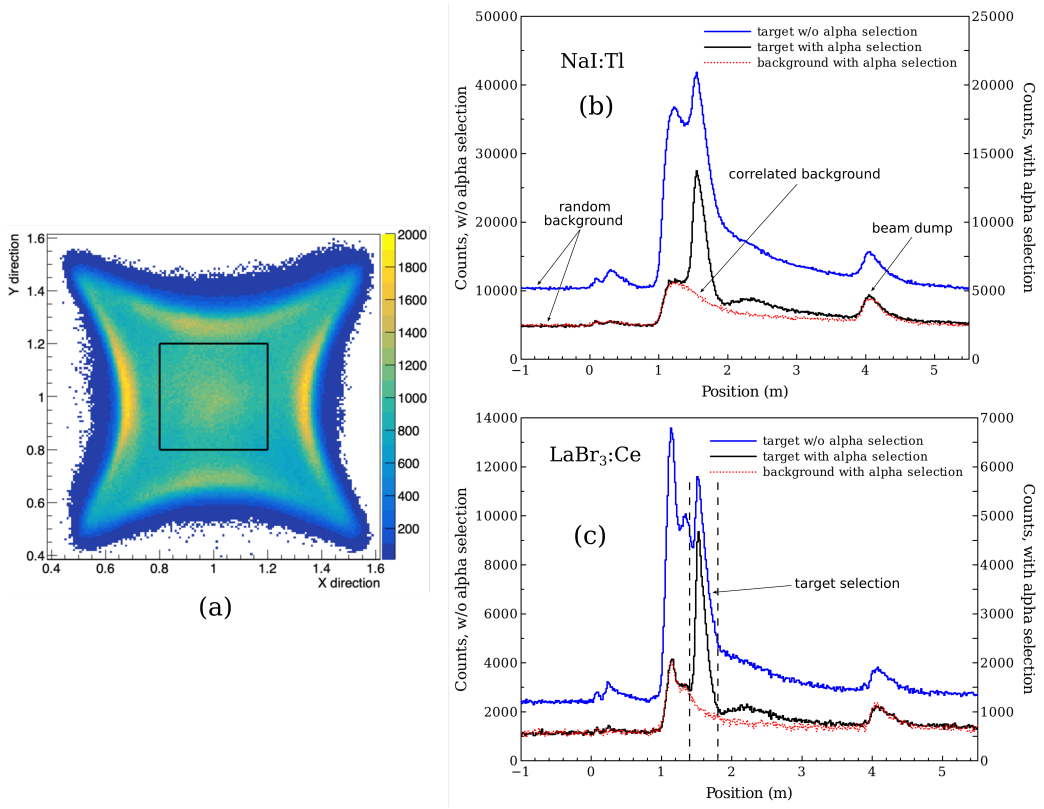

Figure 4: (a) Alpha map in which the black square represents the area corresponding to target events. Panels (b) and (c) show the ToF spectra (position-calibrated) corresponding to the two NaI:Tl and two $LaBr_3$:Ce detectors. A background (acquisition without target) and a measurement with a sample are shown. Right side y-axes give the counts corresponding to the LaBr spectra.

To analyse the random component of the background, we selected on the ToF spectrum, given in Figure 4, the events with a flight path between -5 m and -1 m (the range is not shown in Figure 4). The energy spectra associated to those events acquired with the NaI:Tl and $LaBr_3$:Ce are given in Figure 5a. As can be seen, this component of the background is mainly caused by neutrons interacting in the polyethylene shield, as signed by the presence of peaks at 2.2 MeV (neutron capture on ^{1}H) and 4.4 MeV (inelastic scattering on ^{12}C nuclei). Peaks at 0.847 keV and 1.238 MeV also indicate the presence of iron. The 1.468 MeV (1.436 MeV gamma-ray plus 32 keV characteristic K_α X-ray) peak associated to the $LaBr_3$:Ce internal radioactivity (^{138}La decay) can be also seen on the spectrum. Regarding the correlated component of the background, for each target, the flight-path selection should be applied

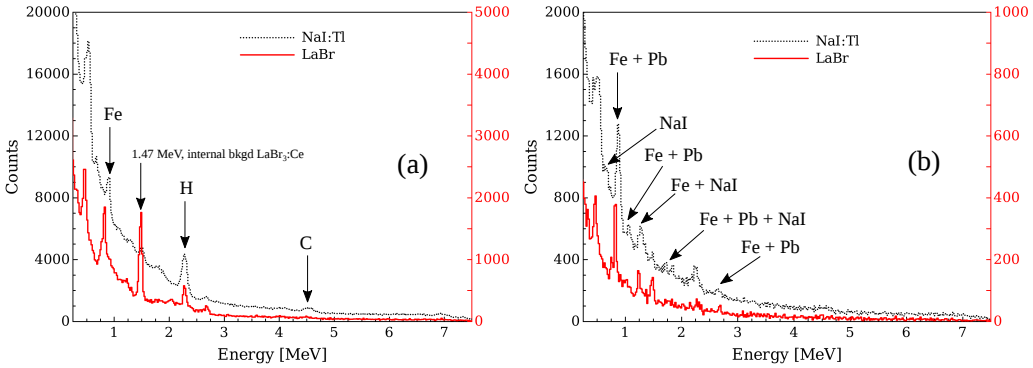

Figure 5: (a) Energy spectrum of the random background. The hydrogen and carbon peaks are seen, the gamma rays are mostly produced in the polyethylene radiological shielding. (b) Energy spectrum of the correlated background, selected on the detectors' holder ToF peak. The iron, lead and sodium peaks are seen, the gamma rays are mostly produced in the detectors themselves and in the detectors' holder.

on the ToF spectrum with and without the target. The NaI:Tl and $LaBr_3$:Ce energy spectra obtained by applying the alpha selection on the case given in Figure 4 are presented in Figure 5b. Fligh-path window was between 1.0 and 2.0 m (corresponding to the position of the detector frame). The peaks observed indicate interactions with the lead shield (Pb), detector frame (Fe) and with the crystals themselves (NaI:Tl).

3.3 Energy spectra of mono-elemental targets

One of the objectives of the experiments at JRC facilities was to build a database of the mono-elemental responses, which are used in the analysis of measurements with unknown targets (unfolding procedure). These measurements allow us to understand the performance and the limits of the detection module. The total intensity (mainly untagged neutrons) of the neutron generator was varied in the tests between 3×10^7 and 7×10^7 s^{-1}. Each acquisition lasted 10 min, which is the foreseen inspection time of a real container in the field. With the neutron generator operating at 5×10^7 s^{-1}, the single count rate in each digitizer channel receiving X, Y and SUM signals was ~ 1 Mcps/channel. However, the DAQ was able to acquire ~ 0.7 Mcps/channel. The coincidence ($\alpha-\gamma$) counting rates for each NaI:Tl, $LaBr_3$:Ce and YAP:Ce detector were ~ 7 kHz, ~ 1.5 kHz and ~ 70 kHz respectively. With such conditions, the quality and quantity of the coincidence rates fulfill the requirements to generate a gamma spectrum with enough statistics to be properly

analyzed. Higher single counting rates of alpha signals cause a worsening of coincidences, increasing random and multiple (one gamma with several alpha signals) coincidences, as proven in [22].

Figure 6 shows the carbon (C), nitrogen (N), oxygen (O), and silicon (Si) responses obtained with graphite blocks, liquid nitrogen (Dewar response subtracted), 6 liters of water and mono-elemental silicon pieces. As an example, Figure 6 shows the data acquired by the two NaI:Tl and the two $LaBr_3$:Ce detectors (one for each side of the detector array). More information about the characteristic energy spectra of these and other elements are given in [23]. There is a perfect agreement between the energy spectra acquired with both kinds of detectors. The better statistics acquired with NaI:Tl detectors is due to their larger size (5" × 5" × 10" instead of 3" × 3" for $LaBr_3$:Ce detectors). However, the excellent energy resolution of the $LaBr_3$:Ce detectors allows to resolve close peaks, as, for example, the 3.6 MeV and 3.8 MeV peaks in the O energy spectrum. Energy resolutions found for the NaI:Tl and $LaBr_3$:Ce detectors at 4.4 MeV (from graphite spectra, Figures 6a) were $(3.8 \pm 0.2)\%$ and $(2.16 \pm 0.05)\%$, respectively. Another important aspect, of the $LaBr_3$:Ce detectors, is the possibility to perform spectroscopy employing a lower energy threshold. Elements like As, Br or I exhibit signatures with energies below 0.5 MeV [14]. In the previous EURITRACK system [11, 10] the energy threshold of NaI:Tl detectors was 0.6 MeV [24]. The addition of the $LaBr_3$:Ce detectors to the system brings better performance for the detection of low-energy gamma signatures (below 0.5 MeV) of specific elements such as arsenic, bromine, or iodine that can be used in chemical warfare.

3.4 Energy spectrum of a simulant

As a final example, Figure 7 presents the gamma energy spectrum of a RDX simulant, acquired with NaI:Tl and $LaBr_3$:Ce detectors. The real RDX chemical formula is $C_3H_6N_6O_6$. On the other hand, the formula of this specific RDX simulant is $Si_3C_3H_6N_6O_6$. Therefore, the silicon contribution to the spectrum has been removed off-line. The main peaks corresponding to C, N and O are indicated in the figure. The excellent energy resolution of the $LaBr_3$:Ce detectors allows to clearly identify the 2.3 MeV, 4.4 MeV and 6.1 MeV gamma photons coming from the N, C and O respectively. In the case of the $LaBr_3$:Ce spectrum also the 1.47 MeV (^{138}La) peak is visible, coming from the detector's internal background.

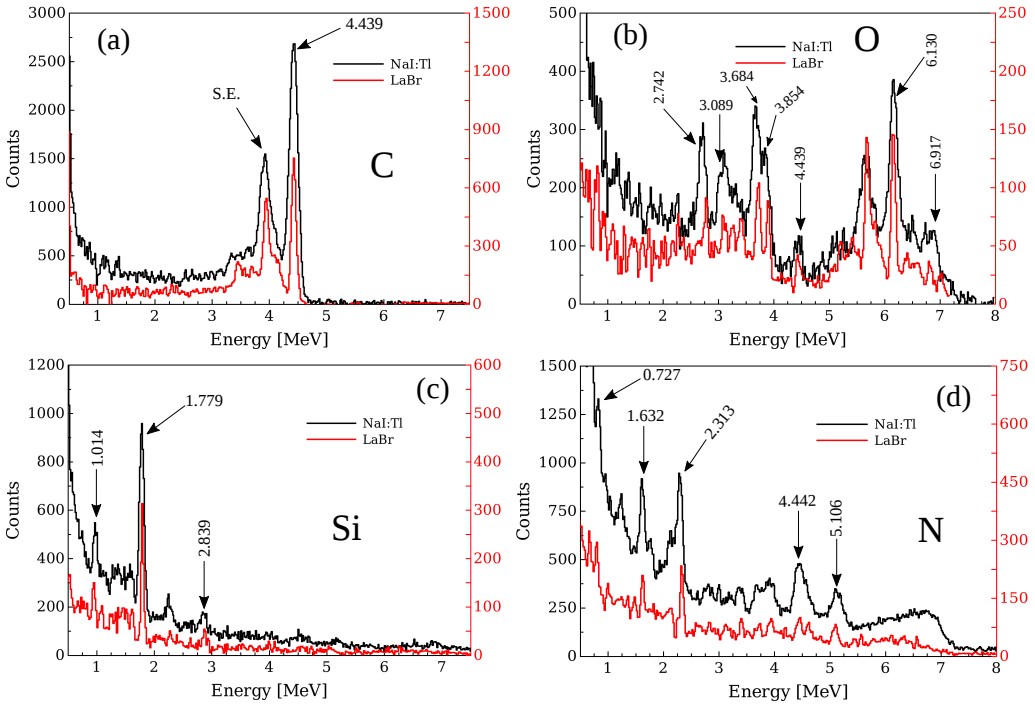

Figure 6: Mono-elemental energy spectra acquired with NaI:Tl and $LaBr_3$:Ce detectors. (a) graphite, (b) water, (c) silicon and (d) nitrogen spectra. Right side y-axes give the counts corresponding to the LaBr spectra.

4 Conclusions

The first integration test of the C-BORD Rapidly Relocatable Tagged Neutron Inspection System (RRTNIS) was performed at the European Commission's Joint Research Centre in Ispra (Italy). The detection module (detectors and nuclear electronics) was integrated with the neutron generator, radiological shielding and mechanics elements. A measurement campaign was carried out, in order to test the whole system's performance. The tests proved that the scintillation detectors (large-size 5" × 5" × 10" NaI:Tl and 3" × 3" $LaBr_3$:Ce) and the newly developed data acquisition system (DAQ) are able to sustain the acquisition rates of the system.

A neutron generator alignment procedure was performed in order to maximize the neutron flux in the beam cone. An estimation of the spatial resolution of the system was obtained. The main technical parameters of the detection module are given in Table 2. The Time-of-Flight (ToF) spectra, acquired with both kinds of detectors, were used to identify the components of background (random and correlated). The main source of random back-

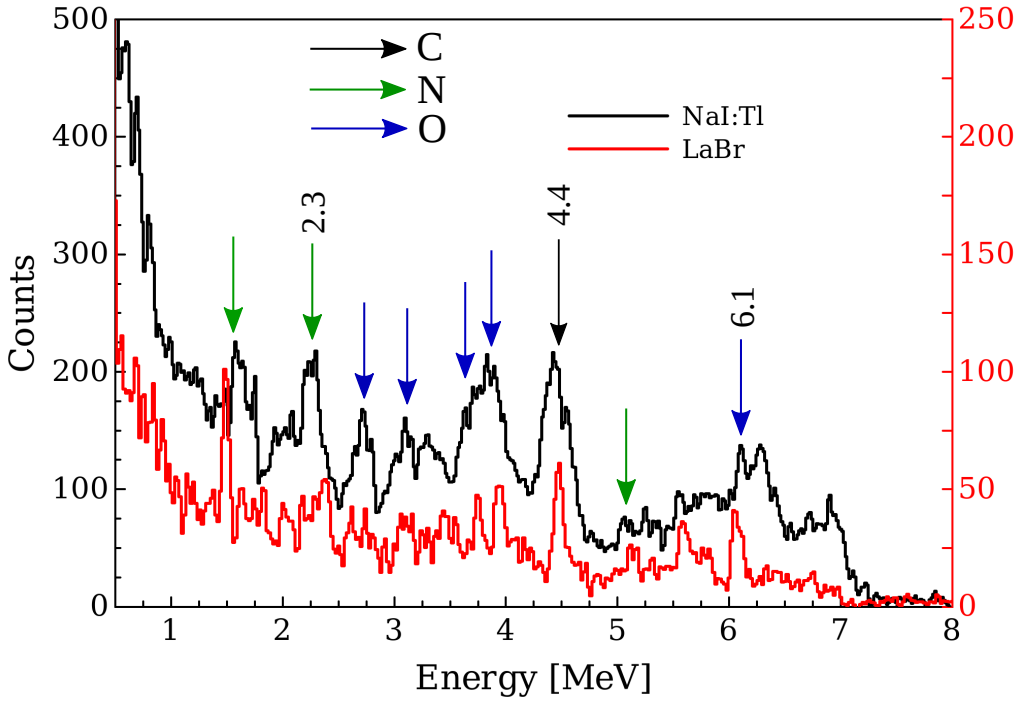

Figure 7: Energy spectra corresponding to a RDX simulant, acquired with NaI:Tl and $LaBr_3$:Ce detectors. Sec. 3.4 describes in details the highlighted peaks. Right side y-axis gives the counts corresponding to the LaBr spectrum.

ground is the interaction of neutrons with the polyethylene shielding, while the correlated background is originated by gamma produced on the detector holder (lead shielding, iron structure) and crystals themselves.

Identification and determination of the position of the targets was done by analyzing the flight-path spectrum. Better position resolution is provided by $LaBr_3$:Ce detectors. A database of mono-elemental targets was built. The addition of $LaBr_3$:Ce detectors in this new system offer better energy resolution and the possibility to detect elements with gamma signatures with energies lower than 0.5 MeV. Finally, a measurement using an explosive simulant was done. Gamma signatures corresponding to the significant elements (C, N and O) were well identified with both kind of detectors.

After this first series of integration tests, the system was transferred to CEA Saclay for a second series of performance tests [5], after which the system was declared ready to perform measurements in the field. Demonstration tests in the Port of Rotterdam (the Netherlands). In the future, we plan to publish the obtained results.

Table 2: Summary of the main technical parameters of the C-BORD Rapidly Relocatable Tagged Neutron Inspection System (RRTNIS). I_n is the neutron generator emission.

	Spatial resolution at 2 m	Energy resolution @4.4 MeV	Coincidence rate $I_n = 5 \times 10^7$ s^{-1}
NaI:Tl	$10 \times 10 \times 10$ cm^3	3.80 %	7 kHz
$LaBr_3$:Ce	$10 \times 10 \times 3$ cm^3	2.16 %	1.5 kHz

5 Acknowledments

We thank Vittorio Forcina, Tatjana Bogucarska, Federica Simonelli and Franco Cioce from JRC, for welcoming the commissioning and first laboratory tests of the RRTNIS.

This work has received funding from the European Union's Horizon 2020 research and innovation programme, under grant agreement No. 653323. This text reflects only the author's views, and the Commission is not liable for any use that may be made of the information contained therein.

References

[1] C. L. Fontana, A. Carnera, M. Lunardon, F. Pino, C. Sada, F. Soramel, L. Stevanato, G. Nebbia, C. Carasco, B. Perot, A. Sardet, G. Sannie, A. Iovene, C. Tintori, K. Grodzicki, M. Moszyński, P. Sibczyński, L. Swiderski, S. Moretto, Detection System of the First Rapidly Relocatable Tagged Neutron Inspection System (RRTNIS), Developed in the Framework of the European H2020 C-BORD Project, Physics Procedia 90 (2017) 279–284. doi:10.1016/j.phpro.2017.09.010.

[2] F. Pino, C. L. Fontana, M. Lunardon, L. Stevanato, C. Sada, A. Carnera, F. Soramel, S. Moretto, G. Nebbia, A. Sardet, C. Carasco, B. Perot, G. Sannie, A. Iovene, C. Tintori, P. Sibczynski, L. Swiderski, K. Grodzicki, M. Moszynski, Advances on the development of the detection system of C-BORD's rapidly relocatable tagged neutron inspection, International Journal of Modern Physics: Conference Series 48 (2018) 1860125. doi:10.1142/S2010194518601254.

[3] A. Sardet, B. Pérot, C. Carasco, G. Sannié, S. Moretto, G. Nebbia, C. Fontana, M. Moszyński, P. Sibczyński, K. Grodzicki, L. Świderski, A. Iovene, C. Tintori, Design of the rapidly relocatable tagged neutron

inspection system of the C-BORD project, in: 2016 IEEE Nuclear Science Symposium, Medical Imaging Conference and Room-Temperature Semiconductor Detector Workshop (NSS/MIC/RTSD), 2016, pp. 1–5. doi:10.1109/NSSMIC.2016.8069693.

[4] A. Sardet, B. Pérot, C. Carasco, G. Sannié, S. Moretto, G. Nebbia, C. Fontana, F. Pino, A. Iovene, C. Tintori, Gamma signatures of the C-BORD Tagged Neutron Inspection System, EPJ Web of Conferences 170 (2018) 07011. doi:10.1051/epjconf/201817007011.

[5] A. Sardet, B. Pérot, C. Carasco, G. Sannié, S. Moretto, G. Nebbia, C. Fontana, F. Pino, Laboratory tests of the C-BORD Rapidly Relocatable Tagged Neutron Inspection System, in: 2019 IEEE Nuclear Science Symposium and Medical Imaging Conference (NSS/MIC), 2019, pp. 1–3. doi:10.1109/NSS/MIC42101.2019.9059950.

[6] A. G. Sébert, J.-P. Poli, Material Classification from Imprecise Chemical Composition : Probabilistic vs Possibilistic Approach, in: 2018 IEEE International Conference on Fuzzy Systems (FUZZ-IEEE), 2018, pp. 1–8. doi:10.1109/FUZZ-IEEE.2018.8491485.

[7] P. Sibczynski, A. Dziedzic, K. Grodzicki, J. Iwanowska-Hanke, Z. Mianowska, M. Moszyñski, L. Swiderski, A. Syntfeld-Każuch, M. Szawł owski, D. Wolski, A. Dołębska, W. Gęsikowski, J. Godlewski, F. Carrel, A. Grabowski, F. Laine, G. Sannie, A. Sari, S. Moretto, C. Fontana, F. Pino, B. Perot, A. Sardet, C. Carasco, C-BORD - an overview of efficient toolbox for high-volume freight inspection, in: 2017 IEEE Nuclear Science Symposium and Medical Imaging Conference (NSS/MIC), 2017, pp. 1–3. doi:10.1109/NSSMIC.2017.8532735.

[8] P. Sibczynski, A. Dziedzic, K. Grodzicki, J. Iwanowska-Hanke, M. Moszyński, L. Swiderski, A. Syntfeld-Każuch, D. Wolski, F. Carrel, A. Grabowski, M. Hamel, F. Laine, A. Sari, A. Iovene, C. Tintori, C. Fontana, F. Pino, New perspectives for undoped CaF2 scintillator as a threshold activation neutron detector, EPJ Web of Conferences 170 (2018) 07012. doi:10.1051/epjconf/201817007012.

[9] B. Perot, C. Carasco, S. Bernard, A. Mariani, J.-L. Szabo, E. Mercier, G. Sannie, G. Viesti, G. Nebbia, S. Pesente, M. Lunardon, S. Moretto, D. Fabris, A. Zenoni, G. Bonomi, A. Donzella, A. Fontana, G. Boghen, V. Valkovic, D. Sudac, M. Moszynski, T. Batsch, M. Gierlik, D. Woski, W. Klamra, P. Isaksson, P. Le Tourneur, M. Lhuissier, A. Colonna, C. Tintori, P. Peerani, V. Sequeira, M. Salvato, Development of the

EURITRACK tagged neutron inspection system, Nuclear Instruments and Methods in Physics Research Section B: Beam Interactions with Materials and Atoms 261 (1-2) (2007) 295–298. doi:10.1016/j.nimb.2007.03.073.

[10] A. Donzella, I. Bodini, A. Zenoni, A. Fontana, B. Perot, S. Bernard, C. Carasco, A. Mariani, D. Sudac, V. Valkovic, Experimental validation of MCNP simulations for the EURITRACK Tagged Neutron Inspection System, Nuclear Instruments and Methods in Physics Research Section B: Beam Interactions with Materials and Atoms 261 (1) (2007) 291–294. doi:10.1016/j.nimb.2007.03.090.

[11] C. Carasco, B. Perot, S. Bernard, A. Mariani, J. L. Szabo, G. Sannie, T. Roll, V. Valkovic, D. Sudac, G. Viesti, M. Lunardon, C. Bottosso, D. Fabris, G. Nebbia, S. Pesente, S. Moretto, A. Zenoni, A. Donzella, M. Moszynski, M. Gierlik, T. Batsch, D. Wolski, W. Klamra, P. Le Tourneur, M. Lhuissier, A. Colonna, C. Tintori, P. Peerani, V. Sequeira, M. Salvato, In-field tests of the EURITRACK tagged neutron inspection system, Nuclear Instruments and Methods in Physics Research Section A: Accelerators, Spectrometers, Detectors and Associated Equipment 588 (3) (2008) 397–405. doi:10.1016/j.nima.2008.01.097.

[12] D. Sudac, S. Pesente, G. Nebbia, G. Viesti, V. Valkovic, Identification of materials hidden inside a container by using the 14MeV tagged neutron beam, Nuclear Instruments and Methods in Physics Research Section B: Beam Interactions with Materials and Atoms 261 (1-2) (2007) 321–325. doi:10.1016/j.nimb.2007.03.088.

[13] S. Pesente, G. Nebbia, G. Viesti, F. Daniele, D. Fabris, M. Lunardon, S. Moretto, K. Nad, D. Sudac, V. Valkovic, Progress in tagged neutron beams for cargo inspections, Nuclear Instruments and Methods in Physics Research Section B: Beam Interactions with Materials and Atoms 261 (1-2) (2007) 268–271. doi:10.1016/j.nimb.2007.03.095.

[14] B. Perot, C. Carasco, C. Deyglun, C. Eleon, W. El Kanawati, A. Mariani, J.-L. Ma, Materials characterisation with the Associated Particle Technique, in: 2012 IEEE Nuclear Science Symposium and Medical Imaging Conference Record (NSS/MIC), IEEE, Anaheim, CA, USA, 2012, pp. 1702–1711. doi:10.1109/NSSMIC.2012.6551402.

[15] C. L. Fontana, M. Lunardon, F. E. Pino, L. Stevanato, A. Carnera, C. Sada, F. Soramel, S. Moretto, A distributed data acquisition system

for signal digitizers with on-line analysis capabilities, in: 2017 IEEE Nuclear Science Symposium and Medical Imaging Conference (NSS/MIC), 2017, pp. 1–5. doi:10.1109/NSSMIC.2017.8533063.

[16] C. L. Fontana, A. Carnera, M. Lunardon, F. E. Pino, C. Sada, F. Soramel, L. Stevanato, S. Moretto, A distributed data acquisition system for nuclear detectors, International Journal of Modern Physics: Conference Series 48 (2018) 1860118. doi:10.1142/S2010194518601187.

[17] C. L. Fontana, M. Lunardon, F. Pino, L. Stevanato, S. Moretto, Resource sharing in nuclear physics laboratory classes: A distributed data acquisition system for experiments with shared resources and data management, in: 25TH INTERNATIONAL CONFERENCE ON THE APPLICATION OF ACCELERATORS IN RESEARCH AND INDUSTRY, Texas, USA, 2019, p. 050024. doi:10.1063/1.5127716.

[18] F. Pino, L. Stevanato, D. Cester, G. Nebbia, L. Sajo-Bohus, G. Viesti, Detecting fast and thermal neutrons with a boron loaded liquid scintillator, EJ-339A, Applied Radiation and Isotopes 92 (2014) 6–11. doi:10.1016/j.apradiso.2014.05.025.

[19] F. Pino, L. Stevanato, D. Cester, G. Nebbia, L. Sajo-Bohus, G. Viesti, The light output and the detection efficiency of the liquid scintillator EJ-309, Applied Radiation and Isotopes 89 (2014) 79–84. doi:10.1016/j.apradiso.2014.02.016.

[20] F. M. Proctor, J. Michaloski, Enhanced machine controller architecture overview, US Department of Commerce, National Institute of Standards and Technology (1993).

[21] T. Staroveski, D. Brezak, T. Udiljak, LinuxCNC – the enhanced machine controller: Application and an overview, Technical Gazette 20 (2013) 1103–1110.

[22] M. Lunardon, C. Bottosso, D. Fabris, S. Moretto, G. Nebbia, S. Pesente, G. Viesti, A. Bigongiari, A. Colonna, C. Tintori, V. Valkovic, D. Sudac, P. Peerani, V. Sequeira, M. Salvato, Front-end electronics and DAQ for the EURITRACK tagged neutron inspection system, Nuclear Instruments and Methods in Physics Research Section B: Beam Interactions with Materials and Atoms 261 (1-2) (2007) 391–395. doi:10.1016/j.nimb.2007.03.072.

[23] B. Perot, C. Carasco, S. Bernard, A. Mariani, J.-L. Szabo, G. Sannie, V. Valkovic, D. Sudac, G. Viesti, M. Lunardon, C. Botosso, G. Nebbia, S. Pesente, S. Moretto, A. Zenoni, A. Donzella, M. Moszynski, M. Gierlik, W. Klamra, P. Le Tourneur, M. Lhuissier, A. Colonna, C. Tintori, P. Peerani, V. Sequeira, M. Salvato, Measurement of 14MeV neutron-induced prompt gamma-ray spectra from 15 elements found in cargo containers, Applied Radiation and Isotopes 66 (4) (2008) 421–434. doi:10.1016/j.apradiso.2007.11.011.

[24] W. El Kanawati, C. Carasco, B. Perot, A. Mariani, A.-C. Raoux, V. Valkovic, D. Sudac, J. Obhodas, M. Baricevic, Gamma-Ray Signatures Improvement of the EURITRACK Tagged Neutron Inspection System Database, IEEE Transactions on Nuclear Science 57 (5) (2010) 2879–2885. doi:10.1109/TNS.2010.2058864.